

Cascade Network with Guided Loss and Hybrid Attention for Finding Good Correspondences

Zhi Chen, Fan Yang, Wenbing Tao*

National Key Laboratory of Science and Technology on Multispectral Information Processing
School of Artificial Intelligence and Automation, Huazhong University of Science and Technology, China
{hust_zhichen, hust_fanyang, wenbingtao}@hust.edu.cn

Abstract

Finding good correspondences is a critical prerequisite in many feature based tasks. Given a putative correspondence set of an image pair, we propose a neural network which finds correct correspondences by a binary-class classifier and estimates relative pose through classified correspondences. First, we analyze that due to the imbalance in the number of correct and wrong correspondences, the loss function has a great impact on the classification results. Thus, we propose a new Guided Loss that can directly use evaluation criterion (Fn-measure) as guidance to dynamically adjust the objective function during training. We theoretically prove that the perfect negative correlation between the Guided Loss and Fn-measure, so that the network is always trained towards the direction of increasing Fn-measure to maximize it. We then propose a hybrid attention block to extract feature, which integrates the Bayesian attentive context normalization (BACN) and channel-wise attention (CA). BACN can mine the prior information to better exploit global context and CA can capture complex channel context to enhance the channel awareness of the network. Finally, based on our Guided Loss and hybrid attention block, a cascade network is designed to gradually optimize the result for more superior performance. Experiments have shown that our network achieves the state-of-the-art performance on benchmark datasets. Our code will be available in <https://github.com/wenbingtao/GLHA>.

Introduction

Two view geometry estimation, i.e., establishing reliable correspondences and estimating relative pose between an image pair, is the fundamental component of many tasks in computer vision, such as Structure from Motion (SfM) (Schonberger and Frahm 2016; Snavely, Seitz, and Szeliski 2006), simultaneous localization and mapping (SLAM) (Benhimane and Malis 2004) and so on. Recently, some methods (Moo Yi et al. 2018; Zhang et al. 2019; Ma et al. 2019) cast the task of finding correct correspondences as a binary classification problem and solve it by neural network. Specifically, these methods first obtain a putative correspondence set of an image pair by extracting local features and matching. Then the network takes the putative set as input

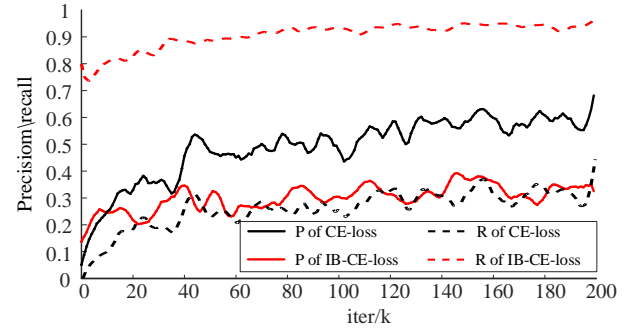


Figure 1: The training curves of different loss functions with same network on YFCC100M&SUN3D dataset. In this dataset, the number ratio of positive and negative samples is about 1 : 10. The imbalance of precision and recall occurs on the network using the above two loss functions.

and divides them into inliers (positive class) and outliers (negative class) and estimates relative pose, i.e., essential matrix (E matrix) (Hartley and Zisserman 2004).

Due to various reasons (e.g., wide-baseline and illumination/scale changes), the number of outliers in the putative correspondence set is much larger than inliers, which usually results in a class imbalance problem of binary classification. As shown in Fig. 1, we train the same network (CN-Net (Moo Yi et al. 2018) is used) with two commonly used loss functions, including cross entropy loss (CE-Loss) and instance balance cross entropy loss (IB-CE-Loss) (Deng et al. 2018) on a class imbalance dataset, and present the training curves of precision and recall. These two loss functions can alleviate the class imbalance problem to some extent in some tasks, such as object classification (He et al. 2016) and segmentation (Chen et al. 2017). However, they lack a direct connection with precision and recall, making the network unable to dynamically adjust the bias of precision and recall. Fig. 1 has demonstrated that, even though the precision and recall have been severely unbalanced during training, the loss functions can not adjust training direction to narrow the gap between precision and recall. In fact, too low either precision or recall will lead to inaccurate relative pose estimation (Hartley and Zisserman 2004). Thus, balanced precision and recall are very important.

*Corresponding author.

The requirement to balance precision and recall can be transformed into a problem of maximizing F_n-measure, an evaluation criterion that considers both precision and recall. In fact, Zhao et. al have already proposed to make F_n-measure differentiable and use it as loss function for salient object detection task (Zhao et al. 2019b). However, when replacing the IB-CE-loss of CN-Net (Moo Yi et al. 2018) with F_n-measure, which has been verified in the subsequent experiments, the network gets a performance degradation. The degradation may be caused by the following two reasons: 1) Some relaxation is necessary to make F_n-measure differentiable to be loss function, which may cause the training becomes a sub-optimization process. 2) The network cannot make use of all the samples, because the TN (true negative) samples are not related with the computation of F_n-measure. In other words, directly using F_n-measure as the loss function may abandon the advantages of cross-entropy loss.

In order to retain the advantage of cross entropy loss while maximizing F_n-measure, we propose a new Guided Loss which keeps the form of the cross entropy and use the F_n-measure as a guidance to adjust the optimization goals dynamically. We theoretically prove that a perfect negative correlation can be established between the loss and F_n-measure by dynamically adjusting the weights of positive and negative classes. Specifically, the perfect negative correlation is that the change in loss is completely opposite to the change in F_n-measure. Thus, with the decrease of the loss, the F_n-measure of the network will increase, so that the network is always trained towards the direction of increasing F_n-measure. By this way, the network maintains the advantage of the cross-entropy loss while maximizing the F_n-measure. It is worth mentioning when establishing the relationship between F_n-measure and loss, no relaxation is required, which is more advantageous than using F_n-measure as loss.

Besides loss function, another challenge is how to better encode global context in the network. Unlike 3D point clouds, not each correspondence contributes to the global context. In contrast, outliers are noises to the global context (Sun et al. 2020). This issue is previously exploited by introducing spatial attention in the network (Plötz and Roth 2018; Sun et al. 2020). These methods learn a weight for each correspondence when encoding global context, so that the network can allow for outliers to be ignored. The key to these approaches is that the weight of outlier must be lower than inlier when encoding global context. However, learning appropriate weight for each correspondence in advance is a chicken-and-egg problem. In the shallow layers of the network, it is hard to learn appropriate weight because the features in these layers are less recognizable. In fact, Lowe Ratio (Lowe 2004), i.e., the side information generated during feature matching, is proved to be powerful prior information to determine the confidence of each point being inlier (Goshen and Shimshoni 2008; Brahmachari and Sarkar 2009). Based on this observation, we propose a Bayesian attentive context normalization (BACN) to mine prior information for better reducing the noise of outliers to global context. The prior can be integrated into the network to better encode global context. Besides, to capture more complex channel-wise context, we generalize the channel-wise atten-

tion (CA) (Hu, Shen, and Sun 2018) operation and reshape it as a point-wise form through group convolution (Cohen and Welling 2016). The BACN and CA are further combined as a hybrid attention block for feature extraction.

Since the proposed Guided Loss can change the network’s bias toward precision and recall by using different F_n-measures (set n as different value) as guidance, we can build a cascade network by the Guided Loss. Specifically, we first train the network through a F_n-measure with big n as the guidance to obtain a coarse result with high recall. So the network keeps as many inliers as possible while filtering out some outliers. After that, F_n-measure with a smaller n can be used as guidance to optimize the coarse result. As n gets smaller, the network gradually leads to a result with higher precision. By gradually optimizing the result from coarse to fine, the network can achieve a better performance than that obtained by one fixed F_n-measure Guided Loss.

In a nutshell, our contribution is threefold: (i) We propose a novel Guided Loss for two-view geometry network. It can establish a direct connection between loss and F_n-measure, so the network can better optimize F_n-measure. (ii) We design a hybrid attention block to better extract global context. It combines a Bayesian attentive context normalization and a channel-wise attention to capture the low-level prior information and channel-wise awareness. (iii) Based on the Guided Loss and hybrid attention block, we design a cascade network for two-view geometry estimation. Experiments show that our network achieves state-of-the-art performance on benchmark datasets.

Related Works

Model fitting methods usually determine inliers by judging whether the raw matches satisfy the fitted epipolar geometric model. The classic RANSAC (Fischler and Bolles 1981) adopts a hypothesize-and-verify pipeline, so do its variants, such as PROSAC (Chum and Matas 2005). Besides, many modifications of RANSAC have been proposed. Some methods (Chum and Matas 2005; Fragoso et al. 2013; Brahmachari and Sarkar 2009; Goshen and Shimshoni 2008) mine prior information to accelerate convergence. Some other methods (Chum, Matas, and Kittler 2003; Barath and Matas 2018) augment the RANSAC by performing a local optimization step on the so-far-the-best model.

Learning Based Methods. Since deep learning has been successfully applied for dealing with unordered data (Qi et al. 2017a,b), learning based methods attract great interest in two-view geometry estimation. CN-Net (Moo Yi et al. 2018) reformulates the mismatch removal task as a binary classification problem. It utilizes a simple Context Normalization (CN) operation to extract global context. Based on CN, some network variants are proposed. NM-Net (Zhao et al. 2019a) employs a simple graph architecture with an affine compatibility-specific neighbor mining approach to mine local context. N^3 -Net (Plötz and Roth 2018) presents a continuous deterministic relaxation of KNN selection and a N^3 block to mine non-local context. OA-Net (Zhang et al. 2019) utilizes an Order-Aware network to build model relation between different nodes. ACN-Net (Sun et al. 2020) introduces spatial attention to two-view geometry network.

Our work is to mine prior information and channel-wise awareness to improve the performance of the network.

Attention Mechanism focuses on perceiving salient areas similar to human visual systems (Vaswani et al. 2017). Non-local neural network (Wang et al. 2018) adopts non-local operation to introduce attention mechanism in feature map. SE-Net (Hu, Shen, and Sun 2018) introduces channel-wise attention mechanism through a Squeeze-and-Excitation block. In order to explore second-order statistics, SAN-Net (Dai et al. 2019) utilizes second-order channel attention (SOCA) operations in their network. In addition to the two dimensional convolution, Wang et. al propose a graph attention convolution (GAC) (Wang et al. 2019) for dealing with point cloud data.

Method

Problem Formulation

Given an image pair, we first extract local features (hand-crafted descriptors such as SIFT (Lowe 2004), or deep learning based descriptors, such as Hard-Net (Mishchuk et al. 2017)) of each image and perform feature matching to establish a set of putative correspondences between them. The coordinates of each correspondence in the putative set are concatenated as the input of our network, as follows:

$$C = [c_1; c_2; \dots, c_N] \in \mathbb{R}^{N \times 4}, c_i = (x_1^i, y_1^i, x_2^i, y_2^i), \quad (1)$$

where N is the number of putative correspondences. (x_1^i, y_1^i) and (x_2^i, y_2^i) are the coordinates of the two feature points of i -th correspondence. The coordinate of each feature point is normalized by camera intrinsics (Moo Yi et al. 2018). The network extracts a feature for each correspondence and determines the probability that a correspondence is inlier based on their features as follows:

$$L = \Phi(C), L \in \mathbb{R}^{N \times 1}, \quad (2)$$

where $\Phi(\cdot)$ is the network with trained parameters. L is the logit values predicted by the network. After that, the network performs a differentiable weighted eight-point algorithm (Moo Yi et al. 2018) on the correspondence to estimate the relative pose (E matrix). as follows:

$$\hat{E} = g(w, C), w = \tanh(\text{ReLU}(L)), \quad (3)$$

$g(\cdot, \cdot)$ is the weighted eight-point algorithm, L is the predicted logit value and \hat{E} is the estimated E matrix.

Guided Loss

The correspondence classification in our network is a binary classification task. In general, the result is evaluated by the Fn-measure (F_n), which considers both precision (P) and recall (R), as follows:

$$F_n = (1 + n^2) \cdot P \cdot R / (n^2 \cdot P + R). \quad (4)$$

When $n > 1$, the Fn-measure is biased in favour of recall and otherwise in favour of precision. When adopting cross entropy loss as objective function, the loss will gradually decrease under the successive optimization. However, there is no guarantee that a drop in the loss will result in

an increase of Fn-measure. Therefore, the network may not be trained towards the direction of optimizing Fn-measure. Based on this observation, we propose a hypothesis, that is, whether the relationship between the cross entropy loss and Fn-measure can be established, so that the decrease of loss will lead to the increase of Fn-measure. This relationship can be expressed in the form of differential as follows:

$$dl \cdot dF_n \leq 0. \quad (5)$$

Specifically, the proposed Guided Loss (l) uses the form of IB-CE-loss as follows:

$$l = -(\lambda \frac{1}{N_{pos}} \sum_{i=1}^{N_{pos}} \log(y_i) + \mu \frac{1}{N_{neg}} \sum_{j=1}^{N_{neg}} \log(1 - y_j)),$$

$$s.t. \quad \lambda + \mu = 1, N_{pos} + N_{neg} = N \quad (6)$$

where N_{pos} and N_{neg} are the number of positive and negative samples. λ and μ are the weights of positive and negative samples. y_i and y_j is the logit value of correspondence i and j respectively. Meanwhile, after forward propagation of the network, all the samples are divided into four categories, including FP (false positive), FN (false negative), TP (true positive) and TN (true negative). Suppose the number of FN and FP samples are X, Y respectively, then the number of TP and TN can be computed as follows:

$$N_{TP} = N_{pos} - X, N_{TN} = N_{neg} - Y, \quad (7)$$

and the precision (P) and recall (R) in Fn-measure (P, R in Eq. 4) can be computed as follows:

$$P = (N_{pos} - X) / (N_{pos} - X + Y),$$

$$R = (N_{pos} - X) / N_{pos}, \quad (8)$$

Thus, Fn-measure is the dependent variable of X and Y according to Eq. 4 and 8. We express the functional relationship between Fn-measure (F_n) and X, Y as follows:

$$F_n = F(X, Y). \quad (9)$$

In order to derive the relationship between Fn-measure and the loss, we also expect to express the loss as the dependent variables of X and Y . In the forward propagation of the network, we can calculate the average loss terms of TP, TN, FP and FN samples respectively, denoted as $l_{TP}, l_{TN}, l_{FP}, l_{FN}$. Then the loss in Eq. 22 can be equivalently calculated as follows:

$$l = \lambda / N_{pos} \cdot \{X \cdot l_{FN} + (N_{pos} - X) \cdot l_{TP}\} + \mu / N_{neg} \cdot \{Y \cdot l_{FP} + (N_{neg} - Y) \cdot l_{TN}\} \quad (10)$$

We compute the derivative forms of loss function (dl) and Fn-measure (dF_n) by X and Y as follows:

$$dl = \partial l_X dX + \partial l_Y dY,$$

$$dF_n = \partial F_X dX + \partial F_Y dY, \quad (11)$$

where ∂l_X and ∂l_Y are the partial derivatives of loss with respect to X and Y , and ∂F_X and ∂F_Y are the partial derivatives of Fn-measure with respect to X and Y . Then, we can draw a sufficient condition of Eq. 5 as follows:

$$\partial F_X / \partial F_Y = \partial l_X / \partial l_Y. \quad (12)$$

Algorithm. The ∂l_X and ∂l_Y can be computed according to Eq. 23 as follows:

$$\begin{aligned}\partial l_X &= \lambda / N_{pos} \cdot (l_{FN} - l_{TP}), \\ \partial l_Y &= \mu / N_{neg} \cdot (l_{FP} - l_{TN}).\end{aligned}\quad (13)$$

Meanwhile, ∂F_X and ∂F_Y can also be calculated by means of numerical derivatives (step 4 in Algorithm 1) in the training process. Obviously, to hold Eq. 12, the weights λ and μ should be dynamically changed during training. This also reveals the problem of IB-CE-Loss using a fixed λ and μ during training. In order to establish a relationship between loss and Fn-measure as Eq. 5, we design a weight adjustment algorithm by making Eq. 12 hold, as follows:

Algorithm 1 Guided Loss

Input: The classification result after forward propagation

Output: Weights of positive and negative samples in loss function (λ and μ)

- 1: **for** $i = 0; i < Batch_size; i++$ **do**
 - 2: Count the number of N_{pos_i} and N_{neg_i} . Count the number TP, TN, FP, FN samples as $N_{TP_i}, N_{FP_i}, N_{TN_i}, N_{FN_i}$, then $X_i = N_{FN_i}, Y_i = N_{FP_i}$.
 - 3: Compute the average loss of TP, TN, FP and FN samples as $l_{TP_i}, l_{TN_i}, l_{FP_i}$ and l_{FN_i} .
 - 4: Compute ∂F_{X_i} and ∂F_{Y_i} : $\partial F_{X_i} = F(X_i + 1, Y_i) - F(X_i, Y_i)$, $\partial F_{Y_i} = F(X_i, Y_i + 1) - F(X_i, Y_i)$
 - 5: s.t. $\lambda_i + \mu_i = 1 \rightarrow$ compute λ_i and μ_i according to Eq. 12, 26 and step 2, 3 and 4
 - 6: **end for**
 - 7: return λ, μ
-

Specifically, when a batch of training data is sent to the network, the first step is forward propagation. After the forward propagation, we can use algorithm 1 to get λ and μ for making Eq. 12 hold. Then we substitute λ and μ into Eq. 22 and perform back propagation.

Hybrid Attention Block

The basic feature extraction block of our network is the proposed hybrid attention block (HAB). As shown in Fig. 2 (a), the input of the HAB is the feature map $f^{N \times C}$ (output of last layer or data points at layer zero), where N is the number of correspondences and C is the number of channels. HAB integrates Bayesian attentive context normalization (BACN), batch normalization (BN) (Ioffe and Szegedy 2015), ReLU and Channel-wise Attention (CA) operations in the structure of Res-Net (He et al. 2016). Specifically, BACN is to normalize each correspondence so that the features of correct and incorrect correspondences are distinguishable. BN is adopted to accelerate network convergence and ReLU function is utilized as an activation function. Finally, the CA operation learns the statistical information on the channel to boost the performance of the network.

Bayesian Attentive Context Normalization. We first briefly introduce how our BACN learns distinguishable features for inliers and outliers. In fact, the inliers are under the constraint of an E matrix while outliers are not (Hartley

and Zisserman 2004). In BACN, a global context is utilized to replace the constraint of E matrix to normalize each correspondence. We use statistical information, i.e., the mean and variance of all features, as the global context. Since the global context is expected to fit the distribution of inliers, we use a weighted mean and variance as the global context, so that the outliers can be ignored by the weight vector. Then, we use the context normalization (Moo Yi et al. 2018) operation to encode feature for each correspondence, as follows:

$$CN(f_i^l) = (f_i^l - u^l) / \sigma^l, \quad (14)$$

where $f_i^l \in \mathbb{R}^C$ is the feature of correspondence i in l -th layer. u^l and σ^l are the weighted mean and variance.

The key to BACN is how to better learn the weight vector for computing weighted mean and variance. In the shallow layers of the network, it's hard to learn appropriate weight vector because the features in these layers are less recognizable. Since Lowe Ratio (Lowe 2004), which is generated during feature matching, is proved useful for determining the confidence of each correspondence being inlier, we expect to use it to make up for the dilemma of weight learning in shallow network. However, the distribution of Lowe Ratio is quite different on different datasets, while independence and identical distribution of features is a very important assumption in neural networks (Bishop 2006). To make better use of Lowe Ratio, we first use the Bayesian Model (Bishop 2006) to convert the it into a probability value. Formally, given a pair of correspondence with Lowe Ratio $r_i \in \mathbb{R}^1$, we consider r_i as a variable and the joint probability distribution function (PDF) can be modeled as:

$$f_r(r_i) = f_{in}(r_i)\alpha + f_{out}(r_i)(1 - \alpha), \quad (15)$$

where $f_{in}(r_i) = f(r_i|r_i \text{ belongs to an inlier})$, $f_{out}(r_i) = f(r_i|r_i \text{ belongs to an outlier})$, and α is the inlier ratio of the putative correspondence set of a specific image pair. Then, the prior probability $p_i(in)$ that the i -th correspondence belongs to inlier can be calculated as follows:

$$p_i(in) = f_{in}(r_i)\alpha / \{f_{in}(r_i)\alpha + f_{out}(r_i)(1 - \alpha)\}. \quad (16)$$

Before training, we obtain the PDF of inlier (f_{in}) and outlier (f_{out}) on the training dataset with ground-truth as empirically PDF. Then for each image pair, we estimate the inlier ratio α using a curve fitting method (Goshen and Shimshoni 2008). Thus we assign a prior probability to each correspondence by Eq. 16.

After obtaining the prior probability for each correspondence, it will be utilized to participate in the calculation of weight vector. The architecture of weight learning is inspired by Bayesian Model (Bishop 2006). The prior probability is similar to the prior probability of Bayesian Model. Meanwhile, as shown in Fig. 2 (a), the input of BACN is followed with two convolution operation to learn a temporary weight vector, which is similar to the likelihood probability of Bayesian Model. The prior probability and the likelihood probability are fused through a feature concatenate operation to generate a feature which encode the information of posterior probability. After that, the posterior feature is followed by two convolution and a softmax operations to produce weight vector. By incorporating prior information, our network is easier to obtain better classification results.

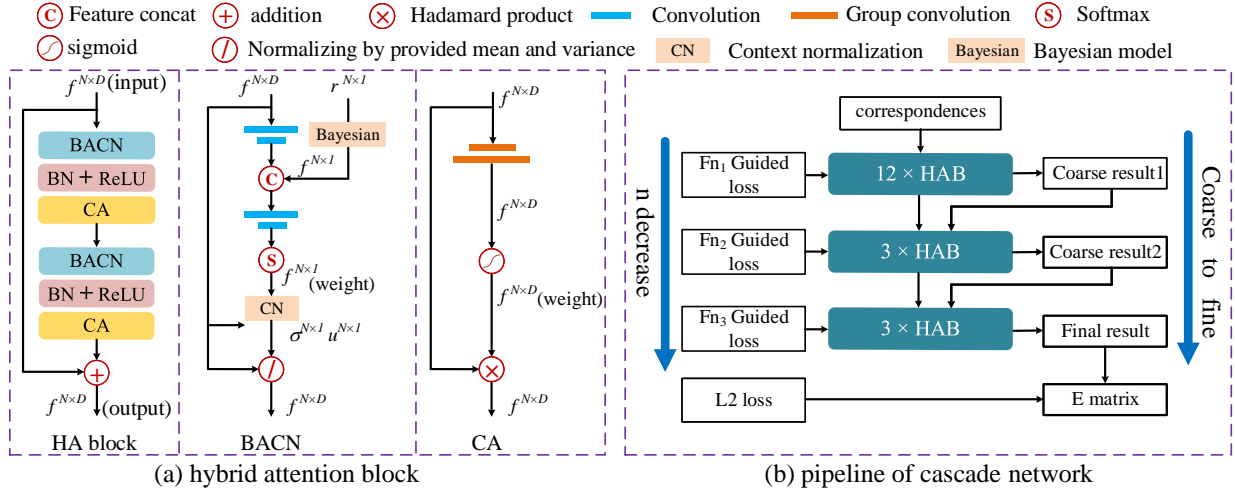


Figure 2: **Network architecture.** (a) The hybrid attention block (HAB) is made up of Bayesian attentive context normalization (BACN), batch normalization, ReLU and channel-wise attention (CA) in a Res-Net (He et al. 2016) architecture. (b) The pipeline of the cascade network.

Channel-wise Attention. The statistics on the channel have been shown to have a significant impact on the network (Hu, Shen, and Sun 2018; Wang et al. 2019). In order to enhance the channel awareness of the network, we introduce channel-wise attention to the HA block. We learn a channel weight vector for each correspondence instead of a weight vector that is shared by all the correspondences to capture complex channel context. When learning the weight vector, group convolution (Cohen and Welling 2016) is used to reduce network computation. Formally, Let $f_i^l \in \mathbb{R}^C$ be the feature of correspondence i in l -th layer, then the CA can be expressed as follows:

$$\text{CA}(f_i^l) = f_i^l * w_i, i = 1, \dots, N, \quad (17)$$

where w_i is obtained by performing two group convolution operations (Cohen and Welling 2016) and a sigmoid function on the feature as shown in Fig. 2 (a).

Cascade Architecture

Since the proposed Guided Loss can flexibly control the bias on precision and recall by using different Fn-measure as guidance, we can naturally build a cascade network by Guided Loss to progressively refine the performance. Specifically, as shown in Fig. 2 (b), we first use a 12-layer hybrid attention blocks as feature extraction module to extract the feature for each correspondence. Then a coarse result (coarse result1 in Fig. 2 (b)) can be obtained through these features by F_{n1} -measure Guided Loss. Then two refinement modules are followed to perform local optimization to refine the coarse result. Each refinement module is made up of a 3-layer HA Block. Different from feature extraction module, the global context in refinement module is extracted from the coarse result of the previous module instead of all of the correspondences. Besides, in order to gradually optimize the coarse result, the loss function will also progressively bias the precision. The coarse result2 is

obtained by F_{n2} -measure Guided Loss, and the final result is obtained by F_{n3} -measure Guided Loss. During training, $n_1 > n_2 > n_3$ holds so that the network gradually obtains result with higher precision. Finally, the E matrix is computed by performing weighted eight-point or RANSAC algorithm on the final result, and it is supervised by a $L2$ -loss. **Loss Function.** We formulate our objective as a combination of two types of loss functions, including classification and regression loss. The whole loss function is as follows:

$$\text{loss} = l_{cls} + \eta_1 l_{cls1} + \eta_2 l_{cls2} + \eta_3 l_{reg}. \quad (18)$$

l_{cls} is related with the final result in Fig. 2, and l_{cls1} and l_{cls2} are related with the coarse result1 and coarse result2 in Fig. 2 respectively. For the regression loss l_{reg} , we use geometric $L2$ -loss for E matrix (Moo Yi et al. 2018) as follows:

$$l_{reg} = \min\{\|\hat{E} \pm E\|\}, \quad (19)$$

where \hat{E} and E are the estimated and ground truth E matrix, respectively.

Experiments

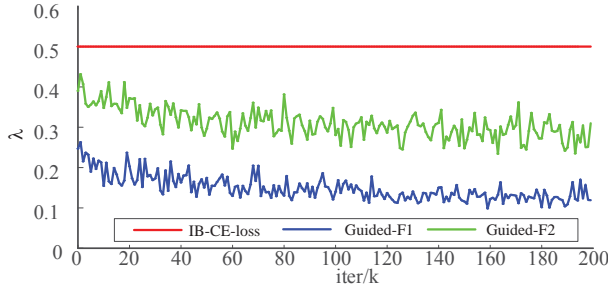
Experimental Setup

Parameter Settings. The network is trained by Adam optimizer (Kingma and Ba 2015) with a learning rate being 10^{-3} and batch size being 16. The iteration times are set to 200k. In Eq. 18, the loss weight η_3 is 0 during the first 20k iteration and then 0.1 later. η_1 and η_2 are set to 0.1 during the whole training. The n_1 , n_2 and n_3 in Fig. 2 are set to 0.3, 0.25 and 0.2 during training, which leads to best relative pose estimation results.

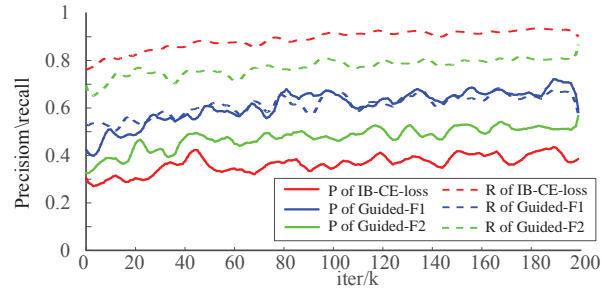
Datasets. We mainly evaluate our method on two benchmark datasets. The first dataset is YFCC100M&SUN3D dataset (Moo Yi et al. 2018). Yi et al. choose 5 scenes from the YFCC100M dataset (Thomee et al. 2016) as outdoor scene and 16 scenes from SUN3D dataset (Xiao, Owens,

Table 1: Comparison with other baselines on YFCC100M&SUN3D and COLMAP dataset. Precision (%), Recall (%), F1-measure (%) and mAP (%) under 5° and 10° (with **weighted eight-point algorithm/with RANSAC**) are reported.

	YFCC100M&SUN3D					COLMAP				
	P	R	F1	mAP 5°	mAP 10°	P	R	F1	mAP 5°	mAP 10°
CN-Net	37.23	73.21	47.08	15.12/33.11	31.87/43.47	27.95	65.63	39.82	11.82/26.89	18.44/30.82
PointNet	27.83	47.23	32.48	12.12/26.31	27.85/33.92	13.60	41.77	27.66	10.41/25.65	17.94/28.76
ACN-Net	41.09	80.96	50.68	27.91/37.18	37.86/47.54	30.13	76.83	38.10	23.15/32.51	27.32/35.88
NM-Net	40.66	71.66	50.74	17.70/34.09	32.80/42.92	31.99	54.48	38.92	20.96/31.72	23.08/33.42
N ³ -Net	40.92	75.34	51.68	14.52/32.65	30.27/42.16	26.88	62.91	33.26	10.90/25.68	16.74/29.77
OA-Net	40.88	72.33	48.58	30.53/37.80	39.84/49.87	37.41	57.74	42.88	26.82/34.57	29.99/37.09
Ours	53.46	70.59	59.67	31.25/41.90	41.52/52.57	42.08	55.21	46.76	27.82/36.83	30.80/39.26



(a) weight λ



(b) Precision and recall

Figure 3: **Training curves.** We train the baseline CN-Net (Moo Yi et al. 2018) with different classification loss on YFCC100M&SUN3D dataset. (a) The weight curve of positive class (λ in Eq. 22). (b) The precision and recall curves on the validation set. We only record the curve of λ because the sum of λ and μ is always 1 during training.

and Torralba 2013) as indoor scene. The ground truth for outdoor and indoor scenes is generated from VSfM (Wu 2013) and KinectFusion (Newcombe et al. 2011). We use their dataset and exact data splits. The second dataset is COLMAP dataset, which is published by Zhao et. al (Zhao et al. 2019a). It contains 16 outdoor scenes. We also use their dataset and exact data splits.

Evaluation Criteria. In the test, we use the trained classification network to get the correspondence classification results, and employ the precision (P), recall (R), F1-measure (F1) (Van Rijsbergen 1974) as the evaluation criteria. Then we perform weighted eight-point (Moo Yi et al. 2018) and RANSAC (Fischler and Bolles 1981) methods as post-processing on the classified correspondence to recover the E matrix between the image pair. In order to evaluate the results of the relative pose estimation, we recover the rotation and translation vectors from the estimated E matrix and report mAP under 5°, 10° as the metrics respectively (Moo Yi et al. 2018; Zhang et al. 2019).

Comparison to Other Baselines

We compare our network with other state-of-the-art methods, including CN-Net (Moo Yi et al. 2018), PointNet (Qi et al. 2017a), ACN-Net (Sun et al. 2020), NM-Net (Zhao et al. 2019a), N³-Net (Plötz and Roth 2018) and OA-Net (Zhang et al. 2019) on both YFCC100M&SUN3D and COLMAP datasets. All the networks are trained with the same setting. Tab. 4 summarizes the correspondence clas-

sification and relative pose estimation results. Our method shows improvement of 15.59% and 6.94% over CN-Net (baseline of our network) in terms of F1-measure on both YFCC100M&SUN3D and COLMAP datasets. In terms of pose estimation results, the mAP of our network is also better than CN-Net by more than 10%. Besides, when compared with another network, our method performs best, especially on correspondence classification task, by nearly 5 to 10 % over the current best approach in terms of F1-measure. These experiments demonstrate that the proposed network behaves favorably to the state-of-the-art approaches.

Ablation studies

HA Block. To demonstrate the performance of HA block, we replace the CN Block in the baseline CN-Net (Moo Yi et al. 2018) with the HA block. Both the Bayesian attentive context normalization (BACN) and channel-wise attention (CA) are tested specifically as Tab. 2. As a comparison, we also replace CN Block with ACN Block (Sun et al. 2020) to train the network. Both of the BACN and CA achieve a better result than ACN, and HA block (BACN + CA) achieves an improvement of about 2% over ACN on both correspondence classification and relative pose estimation results.

Guided Loss. We then replace the original loss of CN-Net with our Guided Loss. As shown in Tab. 2, the proposed Guided Loss (CN-Net + BACN + CA + G-Loss) achieves a better performance over the original loss of CN-Net (CN-Net + BACN + CA) on the terms of F1-measure. It shows

Table 2: Ablation study on YFCC100M&SUN3D datasets. **Precision (%)**, **Recall (%)**, **F1-measure (%)** and **mAP (%)** under 5° and 10° (using **weighted eight-point/RANSAC** as post-processing) are reported. **BACN**: Bayesian attention context normalization. **CA**: channel-wise attention. **ACN**: attentive context normalization (Sun et al. 2020). **G-Loss**: Guided Loss. **No cas**: 18-layer network without cascade architecture. **Cas**: 18-layer network with cascade architecture.

module							result				
CN-Net	BACN	CA	ACN	G-Loss	No-cas	cas	P	R	F1	mAP 5°(%)	mAP 10°(%)
✓							37.23	73.21	47.08	15.12/33.11	31.87/43.47
✓	✓						43.06	79.89	52.63	26.32/36.14	36.41/46.88
✓		✓					42.16	81.22	52.76	26.91/36.85	37.02/47.48
✓	✓	✓					44.08	81.35	53.48	27.83/37.99	37.82/48.29
✓			✓				40.20	80.01	50.48	25.87/35.68	35.66/46.04
✓	✓	✓		✓			51.32	68.27	57.55	29.95/39.88	39.38/50.02
✓	✓	✓		✓	✓		52.09	68.20	57.92	30.32/40.18	40.25/50.51
✓	✓	✓		✓		✓	53.46	70.59	59.67	31.25/41.90	41.52/52.57

Table 3: **Precision (%)**, **Recall (%)**, **F1-measure (%)** and **mAP (%)** 5°, 10° (using **weighted eight-point/RANSAC** as post-processing) on the YFCC100M&SUN3D dataset of different classification loss functions. F-Loss is using Fn-measure as objective function, while G-Loss is the proposed Guided Loss.

	P	R	F1	mAP 5°	mAP 10°
CE-Loss	63.21	46.33	48.67	10.12/26.31	24.85/39.92
IBCE-Loss	37.23	73.21	47.08	15.12/33.11	31.87/43.47
Focal Loss	70.67	41.44	49.67	11.32/27.65	28.94/41.43
F-Loss	44.72	67.43	51.11	10.82/28.90	26.16/39.27
G-Loss	50.62	66.20	56.44	18.52/34.83	33.41/45.64

that the proposed Guided Loss can significantly improve the performance of the classification task. Meanwhile, there is a nearly 2% improvement in the performance of the relative pose task by simply replacing the classification loss without modifying the rest of the network. This is because under the supervision of the proposed Guided Loss, the precision and recall of the classification results are more balanced, which is more conducive to the regression of the E matrix.

Cascade vs. No Cascade. In order to show the performance of the proposed cascade architecture, we first deepen the layers of CN-Net from 12 to 18 and test the result as comparison. Meanwhile, we also train the proposed cascade network, which is also a 18-layer network. As shown in Tab. 2, only increasing the number of network layers, the performance of the network is not significantly improved. The performance of cascade network with the same number of layers is significantly better than non-cascaded networks. It implies that using the Guided Loss in a coarse-to-fine cascade manner can significantly improve network performance.

Guided Loss vs. another loss.

In order to further verify the performance of the proposed Guided Loss, we record the training curves of the weight, precision and recall in Fig. 3. As shown in Fig. 3 (a), λ in the Guided Loss is dynamically changed, while λ in IBCE-Loss is set to fixed value 0.5. As a result, the Guided Loss can achieve a balance between precision and recall, as shown in Fig. 3 (b). Meanwhile, when using F1-measure,

which considers precision and recall equally, as the guidance, the gap between precision and recall is always small. And when using F2-measure, which is more bias towards recall, the recall is always higher than precision. It shows that the result of Guided Loss always accords with the guided Fn-measure, which verifies the effect of the guidance.

Meanwhile, we train the CN-Net (Moo Yi et al. 2018) with the different loss functions (Deng et al. 2018; Zhao et al. 2019b; Lin et al. 2017) and precision, recall, F1-measure and mAP under 5°, 10° are reported in Tab. 3. As discussed in Introduction, when using Fn-measure as objective function, some relaxation has to be made and not all of the samples are utilized for back propagation. Therefore, Fn-Loss does not even perform as well as IB-CE-Loss. For the proposed Guided Loss, the network can achieve a better result than the other loss functions. This is because the Guided Loss can maintain the advantages of IB-CE-Loss while achieving a balance between precision and recall.

Conclusion

In this paper, we present a Guided Loss, which shows a new idea of loss designing. In the proposed Guided Loss, the network is expected to optimize the Fn-measure. Instead of directly using Fn-measure as objective function, we propose to use Fn-measure as the guidance and still adopt the form of cross entropy. Thus, we can maintain the advantage of cross entropy loss while optimizing the Fn-measure. In other tasks, the loss function and evaluation criteria may be different from ours, but the idea of using evaluation criteria to adjust objective function can be used to design more loss functions. Besides, a hybrid attention (HA) block, including a Bayesian attentive context normalization and a channel-wise attention, is proposed for better extracting global context. The Guided Loss and HA Block are combined in a cascade network for two-view geometry tasks. Through extensive experiments, we demonstrate that our network can achieve the state-of-the-art performance on benchmark dataset.

Acknowledgements

This work was supported by the National Natural Science Foundation of China under Grant 61772213, Grant 61991412 and Grant 91748204.

Appendix

Proof of Algorithm 1

Theorem. Given two equations as follows:

$$\partial F_X / \partial F_Y = \partial l_X / \partial l_Y, \quad (20)$$

$$dloss \cdot dFn \leq 0, \quad (21)$$

where ∂l_X and ∂l_Y are the partial derivatives of loss ($loss$) with respect to X and Y , and ∂F_X and ∂F_Y are the partial derivatives of Fn-measure (Fn) with respect to X and Y . $dloss$ and dFn are the derivatives of $loss$ and Fn .

Then, Eq. 20 is a sufficient condition of Eq. 21.

Proof. As introduced in the paper, Fn-measure (Fn) and loss ($loss$) are both the dependent variables of X and Y . Specifically, the form of loss is as follows:

$$l = -(\lambda \frac{1}{N_{pos}} \sum_{i=1}^{N_{pos}} \log(y_i) + \mu \frac{1}{N_{neg}} \sum_{j=1}^{N_{neg}} \log(1 - y_j)),$$

$$s.t. \quad \lambda + \mu = 1, N_{pos} + N_{neg} = N \quad (22)$$

where N_{pos} and N_{neg} are the number of positive and negative samples. We compute the average loss terms of TP , TN , FP and FN samples respectively, denoted as l_{TP} , l_{TN} , l_{FP} , l_{FN} . Then the $loss$ can be transformed as follows:

$$l = \lambda / N_{pos} \cdot \{X \cdot l_{FN} + (N_{pos} - X) \cdot l_{TP}\} + \mu / N_{neg} \cdot \{Y \cdot l_{FP} + (N_{neg} - Y) \cdot l_{TN}\}. \quad (23)$$

Since both the TP and FN samples belong to positive class (ground truth is positive), the loss term of each sample are computed by $-\log(y_i)$ in Eq. 22, where y_i ($0 \leq y_i \leq 1$) is the logit value. In fact, if the logit value of a positive sample (ground truth is positive) is greater than 0.5, then it is a TP sample. And if the logit value is smaller than 0.5, it is a FN sample. Obviously, since $-\log(y_i)$ is a monotone decreasing function, then the loss term of each FN sample is greater than TP sample. Thus, the average loss of FN samples is greater than that of TP samples, i.e.,

$$l_{FN} > l_{TP}. \quad (24)$$

Similarly, the the average loss of FP samples is greater than that of TN samples, i. e.,

$$l_{FP} > l_{TN}. \quad (25)$$

Then, we can compute the partial derivatives of loss with respect to X and Y from Eq. 23, as follows:

$$\begin{aligned} \partial l_X &= \lambda / N_{pos} \cdot (l_{FN} - l_{TP}), \\ \partial l_Y &= \mu / N_{neg} \cdot (l_{FP} - l_{TN}) \end{aligned} \quad (26)$$

According to the constraints of Eq. 24 and 25, we can obtain the following constraints:

$$\partial l_X > 0, \partial l_Y > 0. \quad (27)$$

We then perform the same operations on Fn to obtain the constraints of Fn . Specifically, Fn is related with precision

(P) and recall (R), and P , R are both related with X , Y , as follows:

$$Fn = (1 + n^2) \cdot P \cdot R / (n^2 \cdot P + R), \quad (28)$$

$$\begin{aligned} P &= (N_{pos} - X) / (N_{pos} - X + Y), \\ R &= (N_{pos} - X) / N_{pos}. \end{aligned} \quad (29)$$

According to the compound derivation formula, we can compute the ∂F_X and ∂F_Y as follows:

$$\begin{aligned} \partial F_X &= \partial F_P \cdot \partial P_X + \partial F_R \cdot \partial R_X, \\ \partial F_Y &= \partial F_P \cdot \partial P_Y + \partial F_R \cdot \partial R_Y. \end{aligned} \quad (30)$$

The ∂F_P , ∂F_R , ∂P_X , ∂P_Y all can be computed from Eq. 28 and 29, as follows:

$$\begin{aligned} \partial F_P &= (1 + n^2) \cdot R^2 / (n^2 P + R)^2 \geq 0, \\ \partial F_R &= n^2 (1 + n^2) \cdot P^2 / (n^2 P + R)^2 \geq 0, \\ \partial P_X &= -Y / (N_{pos} - X + Y)^2 \leq 0, \\ \partial P_Y &= -(N_{pos} - X) / (N_{pos} - X + Y)^2 \leq 0, \\ \partial R_X &= -1 / N_{pos} \leq 0, \\ \partial R_Y &= 0, \end{aligned} \quad (31)$$

We can easily obtain the following constraints of ∂F_X and ∂F_Y from Eq. 30, 31:

$$\begin{aligned} \partial F_X &\leq 0, \\ \partial F_Y &\leq 0. \end{aligned} \quad (32)$$

Meanwhile, since Fn-measure (Fn) and loss ($loss$) are both the dependent variables of X and Y , the differential form of $loss$ and Fn in Eq. 21 can be expressed as follows:

$$\begin{aligned} dloss &= \partial l_X dX + \partial l_Y dY, \\ dFn &= \partial F_X dX + \partial F_Y dY, \end{aligned} \quad (33)$$

Thus,

$$\begin{aligned} dloss \cdot dFn &= (\partial l_X dX + \partial l_Y dY) \cdot (\partial F_X dX + \partial F_Y dY) \\ &= \partial l_X \cdot \partial F_X \cdot (dX)^2 + \partial l_Y \cdot \partial F_Y \cdot (dY)^2 \\ &\quad + (\partial l_X \cdot \partial F_Y + \partial l_Y \cdot \partial F_X) \cdot dX \cdot dY \end{aligned} \quad (34)$$

According to the constraints of Eq. 27 and 32, we can further expand Eq. 34 as follows:

$$\begin{aligned} dloss \cdot dFn &= \partial l_X \cdot \partial F_X \cdot (dX)^2 + \partial l_Y \cdot \partial F_Y \cdot (dY)^2 \\ &\quad + (\partial l_X \cdot \partial F_Y + \partial l_Y \cdot \partial F_X) \cdot dX \cdot dY \\ &= \{\partial l_X \cdot \partial F_X \cdot (dX)^2 + \partial l_Y \cdot \partial F_Y \cdot (dY)^2 \\ &\quad - 2\sqrt{\partial l_X \cdot \partial F_X \cdot \partial l_Y \cdot \partial F_Y} \cdot dX \cdot dY\} \\ &\quad + \{(\partial l_X \cdot \partial F_Y + \partial l_Y \cdot \partial F_X) \cdot dX \cdot dY \\ &\quad + 2\sqrt{\partial l_X \cdot \partial F_X \cdot \partial l_Y \cdot \partial F_Y} \cdot dX \cdot dY\} \\ &= -(\sqrt{-\partial l_X \cdot \partial F_X} \cdot dX + \sqrt{-\partial l_Y \cdot \partial F_Y} \cdot dY)^2 \\ &\quad - (\sqrt{-\partial l_X \cdot \partial F_Y} - \sqrt{-\partial l_Y \cdot \partial F_X})^2 \cdot dX \cdot dY \end{aligned} \quad (35)$$

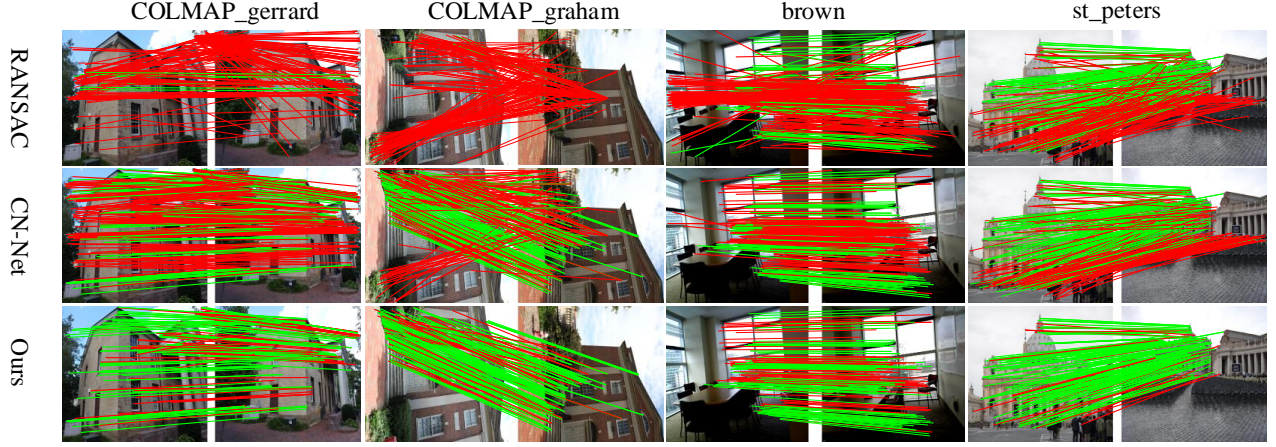


Figure 4: Visual comparison of matching results using RANSAC, CN-Net and our method. Images are taken from YFCC100M&SUN3D and COLMAP datasets. Correspondences are in green if they are inliers, and in red otherwise. **Best viewed in color.**

If Eq. 20 holds, then,

$$\sqrt{-\partial l_X \cdot \partial F_Y} - \sqrt{-\partial l_Y \cdot \partial F_X} = 0, \quad (36)$$

then,

$$\begin{aligned} & d\text{loss} \cdot dFn \\ &= -(\sqrt{-\partial l_X \cdot \partial F_X} \cdot dX + \sqrt{-\partial l_Y \cdot \partial F_Y} \cdot dY)^2 \quad (37) \\ &\leq 0 \end{aligned}$$

Thus, we can proof that Eq. 20 is a sufficient condition of Eq. 21.

Additional Experiments

Guided Loss with other baseline networks. We further analyze our Guided Loss by replacing the classification loss functions of other models with Guided Loss. We first train three recent networks, including CN-Net (Moo Yi et al. 2018), ACN-Net (Sun et al. 2019) and NM-Net (Zhao et al. 2019a), with their original classification loss. Then we replace their classification loss with our Guided Loss. The results are reported in Tab. 4. Each network with the supervision of our loss can lead to a result with more balanced precision and recall and a higher F1-measure. As a result, the each network increase the mAP by 1-3% without modifying anything.

Parameter n of Guided Loss. Our Guided Loss is designed to build a perfect negative correlation relationship between cross entropy loss and Fn-measure for better optimizing Fn-measure. To verify that our guidance actually works, we train the CN-Net (Moo Yi et al. 2018) with different Fn-measure Guided Loss, respectively. Meanwhile, we also train the CN-Net with the cross entropy loss (CE-Loss) and Instance Balance cross entropy loss (Deng et al. 2018; Moo Yi et al. 2018) (IB-CE-Loss). The classification result are shown in Tab. 5. We record the precision (P), recall (R), and five Fn-measures ($n = 0.5, 1, 1.5, 2, 2.5$ respectively) of the classification results on test dataset. As shown in Tab.

Table 4: The results of three networks with both their original classification loss (without "+" in the table) and our F2-measure Guided Loss (with "+" in the table). **Precision (%)**, **Recall (%)**, **F1-measure (%)** and **mAP (%)** 5°, 10° (using **weighted eight-point/RANSAC** as post-processing) on the YFCC100M&SUN3D dataset are reported.

	P	R	F1	mAP 5°	mAP 10°
CN-Net	37.23	73.21	47.08	15.12/33.11	31.87/43.47
CN-Net +	50.62	66.20	56.44	18.52/34.83	33.41/45.64
ACN-Net	40.20	80.01	50.48	25.87/35.68	35.66/46.04
ACN-Net +	49.88	66.57	57.55	27.32/37.13	36.98/47.65
NM-Net	40.66	71.66	50.74	17.70/34.09	32.80/42.92
NM-Net +	46.72	65.44	55.68	19.89/36.79	34.32/44.02

Table 5: The classification results of CN-Net (Moo Yi et al. 2018) with different loss functions on YFCC100M&SUN3D dataset. **G-Fn:** ($n = 0.5, \dots, 2.5$) is the Guided Loss with the guidance of different Fn-measure. **IB-CE:** instance balance cross entropy loss. **CE:** cross entropy loss. The precision (P), recall (R) and 5 Fn-measure (Fn) are reported.

	P	R	F0.5	F1	F1.5	F2	F2.5
G-F0.5	64.5	51.1	60.5	56.0	53.8	52.7	52.2
G-F1	56.8	57.8	57.2	57.3	55.9	56.7	56.6
G-F1.5	48.6	64.6	50.6	54.3	58.2	59.6	60.9
G-F2	47.4	67.3	49.8	54.3	57.2	60.9	62.6
G-F2.5	43.6	69.2	46.6	52.2	57.1	60.5	63.8
IB-CE	37.2	77.1	40.0	47.1	53.8	59.4	62.9
CE	63.2	48.3	56.7	52.1	51.1	50.7	50.5

5, with the guidance of a specific Fn-measure, our Guided Loss can achieve the best performance on this measurement. It shows the direct guidance of our loss. We can choose the corresponding Fn-measure to guide the loss according to the requirements of precision and recall of different tasks.

Visual Result. In order to show the classification result of our network, we visualize the matching results of RANSAC (Fischler and Bolles 1981), CN-Net (Moo Yi et al. 2018) and our network in Fig. 4.

References

- Barath, D.; and Matas, J. 2018. Graph-cut RANSAC. In *Proceedings of the IEEE Conference on Computer Vision and Pattern Recognition*, 6733–6741.
- Benhimane, S.; and Malis, E. 2004. Real-time image-based tracking of planes using efficient second-order minimization. In *2004 IEEE/RSJ International Conference on Intelligent Robots and Systems (IROS)(IEEE Cat. No. 04CH37566)*, volume 1, 943–948. IEEE.
- Bishop, C. M. 2006. *Pattern Recognition and Machine Learning (Information Science and Statistics)*. Berlin, Heidelberg: Springer-Verlag.
- Brahmachari, A. S.; and Sarkar, S. 2009. BLOGS: Balanced local and global search for non-degenerate two view epipolar geometry. In *2009 IEEE 12th International Conference on Computer Vision*, 1685–1692. IEEE.
- Chen, L.-C.; Papandreou, G.; Kokkinos, I.; Murphy, K.; and Yuille, A. L. 2017. Deeplab: Semantic image segmentation with deep convolutional nets, atrous convolution, and fully connected crfs. *IEEE transactions on pattern analysis and machine intelligence* 40(4): 834–848.
- Chum, O.; and Matas, J. 2005. Matching with PROSAC: progressive sample consensus. In *2005 IEEE Computer Society Conference on Computer Vision and Pattern Recognition (CVPR'05)*, volume 1, 220–226. IEEE.
- Chum, O.; Matas, J.; and Kittler, J. 2003. Locally optimized RANSAC. In *Joint Pattern Recognition Symposium*, 236–243. Springer.
- Cohen, T.; and Welling, M. 2016. Group equivariant convolutional networks. In *International conference on machine learning*, 2990–2999.
- Dai, T.; Cai, J.; Zhang, Y.; Xia, S.-T.; and Zhang, L. 2019. Second-order Attention Network for Single Image Super-Resolution. In *Proceedings of the IEEE Conference on Computer Vision and Pattern Recognition*, 11065–11074.
- Deng, D.; Liu, H.; Li, X.; and Cai, D. 2018. Pixellink: Detecting scene text via instance segmentation. In *Thirty-Second AAAI Conference on Artificial Intelligence*.
- Fischler, M. A.; and Bolles, R. C. 1981. Random sample consensus: a paradigm for model fitting with applications to image analysis and automated cartography. *Communications of the ACM* 24(6): 381–395.
- Fragoso, V.; Sen, P.; Rodriguez, S.; and Turk, M. 2013. EVSAC: accelerating hypotheses generation by modeling matching scores with extreme value theory. In *Proceedings of the IEEE International Conference on Computer Vision*, 2472–2479.
- Goshen, L.; and Shimshoni, I. 2008. Balanced exploration and exploitation model search for efficient epipolar geometry estimation. *IEEE Transactions on Pattern Analysis and Machine Intelligence* 30(7): 1230–1242.
- Hartley, R.; and Zisserman, A. 2004. *Multiple View Geometry in Computer Vision*. Cambridge University Press, 2 edition.
- He, K.; Zhang, X.; Ren, S.; and Sun, J. 2016. Deep residual learning for image recognition. In *Proceedings of the IEEE conference on computer vision and pattern recognition*, 770–778.
- Hu, J.; Shen, L.; and Sun, G. 2018. Squeeze-and-excitation networks. In *Proceedings of the IEEE conference on computer vision and pattern recognition*, 7132–7141.
- Ioffe, S.; and Szegedy, C. 2015. Batch normalization: Accelerating deep network training by reducing internal covariate shift. *arXiv preprint arXiv:1502.03167*.
- Kingma, D. P.; and Ba, J. 2015. Adam: A method for stochastic optimization. In *Proceedings of the International Conference on Learning Representations*.
- Lin, T.-Y.; Goyal, P.; Girshick, R.; He, K.; and Dollár, P. 2017. Focal loss for dense object detection. In *Proceedings of the IEEE international conference on computer vision*, 2980–2988.
- Lowe, D. G. 2004. Distinctive image features from scale-invariant keypoints. *International journal of computer vision* 60(2): 91–110.
- Ma, J.; Jiang, X.; Jiang, J.; Zhao, J.; and Guo, X. 2019. Lmr: Learning a two-class classifier for mismatch removal. *IEEE Transactions on Image Processing*.
- Mishchuk, A.; Mishkin, D.; Radenovic, F.; and Matas, J. 2017. Working hard to know your neighbor’s margins: Local descriptor learning loss. In *Advances in Neural Information Processing Systems*, 4826–4837.
- Moo Yi, K.; Trulls, E.; Ono, Y.; Lepetit, V.; Salzmann, M.; and Fua, P. 2018. Learning to find good correspondences. In *Proceedings of the IEEE Conference on Computer Vision and Pattern Recognition*, 2666–2674.
- Newcombe, R. A.; Izadi, S.; Hilliges, O.; Molyneaux, D.; Kim, D.; Davison, A. J.; Kohi, P.; Shotton, J.; Hodges, S.; and Fitzgibbon, A. 2011. KinectFusion: Real-time dense surface mapping and tracking. In *2011 10th IEEE International Symposium on Mixed and Augmented Reality*, 127–136. IEEE.
- Plötz, T.; and Roth, S. 2018. Neural Nearest Neighbors Networks. In *Advances in Neural Information Processing Systems (NeurIPS)*.
- Qi, C. R.; Su, H.; Mo, K.; and Guibas, L. J. 2017a. Pointnet: Deep learning on point sets for 3d classification and segmentation. In *Proceedings of the IEEE Conference on Computer Vision and Pattern Recognition*, 652–660.

- Qi, C. R.; Yi, L.; Su, H.; and Guibas, L. J. 2017b. Pointnet++: Deep hierarchical feature learning on point sets in a metric space. In *Advances in neural information processing systems*, 5099–5108.
- Schonberger, J. L.; and Frahm, J.-M. 2016. Structure-from-motion revisited. In *Proceedings of the IEEE Conference on Computer Vision and Pattern Recognition*, 4104–4113.
- Snavely, N.; Seitz, S. M.; and Szeliski, R. 2006. Photo tourism: exploring photo collections in 3D. In *ACM transactions on graphics (TOG)*, volume 25, 835–846. ACM.
- Sun, W.; Jiang, W.; Trulls, E.; Tagliasacchi, A.; and Yi, K. M. 2019. Attentive Context Normalization for Robust Permutation-Equivariant Learning. *arXiv preprint arXiv:1907.02545*.
- Sun, W.; Jiang, W.; Trulls, E.; Tagliasacchi, A.; and Yi, K. M. 2020. ACNe: Attentive Context Normalization for Robust Permutation-Equivariant Learning. In *Proceedings of the IEEE/CVF Conference on Computer Vision and Pattern Recognition*, 11286–11295.
- Thomee, B.; Shamma, D. A.; Friedland, G.; Elizalde, B.; Ni, K.; Poland, D.; Borth, D.; and Li, L.-J. 2016. YFCC100M: The new data in multimedia research. *Communications of the ACM* 59(2): 64–73.
- Van Rijsbergen, C. J. 1974. Foundation of evaluation. *Journal of documentation* 30(4): 365–373.
- Vaswani, A.; Shazeer, N.; Parmar, N.; Uszkoreit, J.; Jones, L.; Gomez, A. N.; Kaiser, Ł.; and Polosukhin, I. 2017. Attention is all you need. In *Advances in neural information processing systems*, 5998–6008.
- Wang, L.; Huang, Y.; Hou, Y.; Zhang, S.; and Shan, J. 2019. Graph Attention Convolution for Point Cloud Semantic Segmentation. In *Proceedings of the IEEE Conference on Computer Vision and Pattern Recognition*, 10296–10305.
- Wang, X.; Girshick, R.; Gupta, A.; and He, K. 2018. Non-local neural networks. In *Proceedings of the IEEE Conference on Computer Vision and Pattern Recognition*, 7794–7803.
- Wu, C. 2013. Towards linear-time incremental structure from motion. In *2013 International Conference on 3D Vision-3DV 2013*, 127–134. IEEE.
- Xiao, J.; Owens, A.; and Torralba, A. 2013. SUN3D: A Database of Big Spaces Reconstructed Using SfM and Object Labels 1625–1632.
- Zhang, J.; Sun, D.; Luo, Z.; Yao, A.; Zhou, L.; Shen, T.; Chen, Y.; Quan, L.; and Liao, H. 2019. Learning Two-View Correspondences and Geometry Using Order-Aware Network. *arXiv preprint arXiv:1908.04964*.
- Zhao, C.; Cao, Z.; Li, C.; Li, X.; and Yang, J. 2019a. NM-Net: Mining Reliable Neighbors for Robust Feature Correspondences. In *Proceedings of the IEEE Conference on Computer Vision and Pattern Recognition*, 215–224.
- Zhao, K.; Gao, S.; Wang, W.; and Cheng, M.-M. 2019b. Optimizing the f-measure for threshold-free salient object detection. In *Proceedings of the IEEE International Conference on Computer Vision*, 8849–8857.